

## Hot-electron bistability in quantum-dot structures

S. M. Goodnick

*Department of Electrical and Computer Engineering, Oregon State University, Corvallis, Oregon 97331*

J. C. Wu and M. N. Wybourne

*Physics Department, University of Oregon, Eugene, Oregon 97403*

Doran D. Smith

*Army Research Laboratory, Electronics and Power Sources Directorate, MS, AMSRL-EP-EF, Ft. Monmouth, New Jersey 07703-5601*

(Received 17 June 1993)

We present a theoretical analysis of hot-electron bistability in quantum-dot structures. An energy balance approach is used to demonstrate the existence of negative differential conductance due to thermal runaway of the carriers in the dot structure. This runaway is shown to arise from heating of carriers in the quantum dot by incident electrons injected over the barrier of the input constriction. Excellent agreement is obtained with recent experimental evidence of bistability in the current-voltage characteristics of laterally confined quantum dots [J. C. Wu, M. N. Wybourne, C. Berven, S. M. Goodnick, and D. D. Smith, *Appl. Phys. Lett.* **61**, 1 (1992)].

Most studies of quantum waveguide and other interference effects have focused on their near equilibrium conductance properties (see, for example, the review in Ref. 2). However, relatively little has been reported concerning hot-electron phenomena<sup>3,4</sup> in mesoscopic systems. Recently we reported the observation of negative differential conductance (NDC) in the current-voltage characteristics of a lateral double constriction point contact structure.<sup>1</sup> There, a quantum dot with variable size and coupling to the external contact regions was formed using electrostatic confinement. A schematic top view of the gate electrode structure superimposed on a modulation doped two-dimensional electron gas (2DEG) structure is shown in the inset of Fig. 1. When the gate electrodes are biased so as to deplete carriers under them, a bias applied through Ohmic contacts between the 2DEG's (source and drain) on either side of the cavity forces current to traverse the path shown schematically in Fig. 1. The current-voltage characteristics show

a marked *S*-type NDC between high and low impedance states. The transition from high to low impedance is a strong function of gate bias, with the threshold voltage for switching increasing with increasing negative bias.

*S*-type NDC has also been observed in two terminal semiconductor heterolayer structures.<sup>5-9</sup> For these devices, it was established that NDC occurs through carrier heating by hot electrons injected over the heterojunction barriers. A model was presented using an energy balance approach for injected electrons thermalizing with cold electrons trapped between heterojunction barriers which qualitatively agrees with the experimental current-voltage characteristics.<sup>10,11</sup> This model for hot-electron instabilities in the so-called heterostructure hot-electron diode was further supported by Monte Carlo simulation of the structure.<sup>12</sup>

In the present paper, we show that the controllable switching behavior in lateral double constriction point contact structures can be explained by a similar energy balance approach for heating of electrons trapped in the cavity region of the dot. Using physically reasonable model parameters, the calculated current-voltage characteristics predict *S*-type NDC in good agreement with the experimental data of Wu *et al.*<sup>1</sup> The model is also used to predict the evolution of the electron temperature with the current through the device.

To begin, consider the potential barriers encountered by electrons as they traverse the path shown by the inset of Fig. 1. At the points labeled *A* and *B*, the input and output to the quantum dot, the potential is raised due to depletion of the 2DEG by the reverse biased electrodes. With zero applied source-drain bias, an activation barrier  $\phi_0$  exists between the electrons in the 2DEG and the quantum dot due to energy quantization in the one-dimensional channel as well as the electrostatic potential associated with the depletion regions of the gate elec-

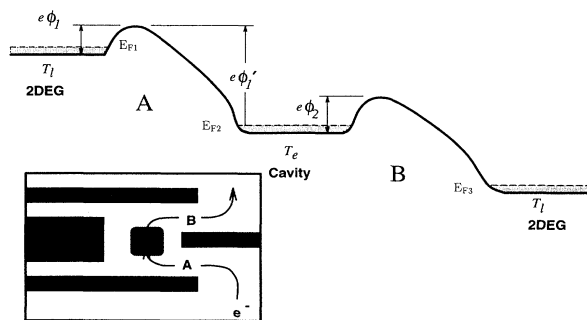


FIG. 1. Schematic of the energy band profile for a lateral double constriction quantum dot. The inset shows the lateral gate pattern and electron trajectory through the structure.

trodes. A schematic of the potential along the current path is shown in Fig. 1 for an applied bias  $V_{sd}$  across the structure. The Fermi energies shown there,  $E_{F1}$ ,  $E_{F2}$ , and  $E_{F3}$ , are split unequally by the applied bias according to

$$\frac{1}{e}(E_{F1} - E_{F2}) = \frac{V_{sd}}{2} + \frac{Q}{C}, \quad (1)$$

$$\frac{1}{e}(E_{F2} - E_{F3}) = \frac{V_{sd}}{2} - \frac{Q}{C}, \quad (2)$$

where  $C$  is the charging capacitance between the dot and the 2DEG on either side of the dot, and  $Q = e(N_0 - N)$  is the excess charge in the dot, where  $N$  is the number of electrons and  $N_0$  the equilibrium number. Under bias, the input barrier  $\phi_1$  is decreased compared to the zero bias barrier  $\phi_0$  as

$$\phi_1 = \phi_0 - \left( \frac{V_{sd}}{2} + \frac{Q}{C} \right) / \alpha \quad (3)$$

while the output barrier  $\phi_2$  decreases as

$$\phi_2 = \phi_0 - \left( \frac{V_{sd}}{2} - \frac{Q}{C} \right) / \alpha, \quad (4)$$

where  $\phi_1$  and  $\phi_2$  are defined in Fig. 1 and the barrier modulation factor  $\alpha$  depends on the abruptness of the barrier. For a perfectly abrupt barrier,  $\alpha$  would be infinite (neglecting any image lowering effects). In the present case, the rise of the potential barrier occurs roughly over the length of the depletion region around the gate electrodes which is on the order of the channel width  $W$ . In the structure of Wu *et al.*,<sup>1</sup> the length of the 1D channels at the constriction are the same as the width, thus  $\alpha \approx 3$ . Finally, an important parameter governing heating of the cavity electrons is the injection energy  $e\phi_1'$  shown in Fig. 1, which is related to the applied bias as

$$\phi_1' = \phi_0 + \left( \frac{V_{sd}}{2} + \frac{Q}{C} \right) \left( 1 - \frac{1}{\alpha} \right). \quad (5)$$

To derive an energy balance model for the system, we first assume that the dimensions of the quantum dot are sufficiently large that the electrons can be treated as a finite extent 2DEG. A second assumption is that electrons injected over the input barrier  $A$  thermalize through carrier-carrier scattering with the cavity electrons before being thermionically emitted over the second barrier. Thus ballistic transport from barrier  $A$  over barrier  $B$  is assumed to be minimal. Tunneling through the barriers is also neglected. Current into and out of the cavity is thus assumed to be limited by thermionic emission over barriers. At the first barrier, the current is given by

$$I = eWv_l kT_l D_0 \left( e^{n_s/D_0 kT_l} - 1 \right) e^{-e\phi_1/kT_l}, \quad (6)$$

where  $W$  is the width of the constriction,  $T_l$  is the lattice temperature,  $v_l = \sqrt{kT_l/2\pi m^*}$  is the mean velocity of the 2DEG incident on the constriction,  $D_0 = m^*/\pi\hbar^2$  is the 2D density of states, and  $n_s$  is the 2DEG concen-

tration. In Eq. (6), the distribution at the top of the barrier is assumed nondegenerate. The thermionic current flowing from the dot back into region 1 was found to be negligible at all but the highest cavity temperatures, and was thus neglected. Therefore, Eq. (6) gives the input barrier  $\phi_1$  once the current  $I$  is chosen. Similarly, the current flowing through the second constriction  $B$  is given by

$$I = eWv_e kT_e D_0 \left( e^{N/AD_0 kT_e} - 1 \right) e^{-e\phi_2/kT_e}, \quad (7)$$

where  $T_e$  is the electron temperature of a heated Maxwell-Boltzmann distribution in the cavity as indicated in Fig. 1,  $v_e$  is the same as  $v_l$  for  $T = T_e$ ,  $A$  is the undepleted area of the dot, and again the reverse flux of carriers is negligible for the situation shown. Under steady-state conditions, the two currents given by Eqs. (6) and (7) are identical.

A third equation is the electron energy balance equation in the cavity,

$$I \left( \phi_1' + \frac{kT_l}{e} - \phi_2 - \frac{kT_e}{e} \right) = N \left\langle \frac{\partial E}{\partial t} \right\rangle_{\text{coll}}. \quad (8)$$

The energy loss rate for electrons in  $\text{Al}_x\text{Ga}_{1-x}\text{As}/\text{GaAs}$  2D gas structures has been reported over a broad range of carrier temperatures by Shah *et al.* using photoluminescence spectroscopy.<sup>13</sup> The energy loss rate per electron in Eq. (8) may be fit to their data assuming polar-optical and acoustic-phonon scattering dominate as

$$\left\langle \frac{\partial E}{\partial t} \right\rangle_{\text{coll}} \approx \frac{\hbar\omega_0}{\tau_{\text{pop}}} e^{-\hbar\omega_0/kT_e} + \frac{k(T_e - T_l)}{\tau_{\text{ac}}}, \quad (9)$$

where  $\omega_0$  is the longitudinal-optical phonon energy,  $\tau_{\text{pop}}$  is the effective polar-optical phonon emission time, and  $\tau_{\text{ac}}$  is the acoustic-phonon energy relaxation time.

Controversy exists as to the actual deformation potential which fits the experimental data of various groups in the regime where acoustic phonons dominate the loss rate.<sup>14-16</sup> Part of this discrepancy is attributable to additional energy loss from collective excitations as shown by Kawamura *et al.*<sup>17</sup> Using a value for the effective acoustic deformation potential of  $D = 16$  eV in the energy loss rate expression given by Daniels, Ridley, and Emeny<sup>18</sup> results in  $\tau_{\text{ac}} = 1.8$  ns, which gives a reasonable fit to the data of Shah *et al.*<sup>13</sup> For polar-optical scattering, the nominal value of  $\tau_{\text{pop}}$  is 130 fs. However, nonequilibrium LO phonons reduce the actual energy loss rate in quantum well systems (for a recent review, see Ref. 19), which is necessary to account for the data of Shah *et al.* Taking an effective scattering time of  $\tau_{\text{pop}} = 2$  ps gives good agreement with the data of Shah *et al.* over a wide range of electron temperatures.

Once the current  $I$  is chosen, the three equations for the current and energy loss rate, Eqs. (6), (7), and (8), together with the auxiliary equations (3), (4), and (5), are solved simultaneously for the source drain voltage  $V_{sd}$ , the dot charge  $Q$ , and the electron temperature  $T_e$ . Figure 2 shows the calculated results using the above formalism compared to experimental data from Wu *et*

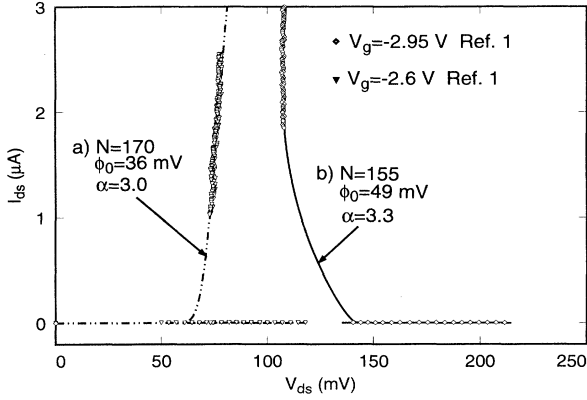


FIG. 2. Calculated current voltage characteristics for two different sets of data from Ref. 1. Fit (a) corresponds to the experimental data for  $V_g = -2.6$  V while (b) corresponds to  $V_g = -2.95$  V. Switching for both the experimental and theoretical calculation occurs along the  $x$  axis. The theory in both cases follows the maximum extent of the data of Wu *et al.*

$al.$ <sup>1</sup> for two different gate bias conditions at  $T_l = 4.2$  K. The 2DEG density was taken to be  $3.7 \times 10^{11}/\text{cm}^2$  as determined experimentally from magnetotransport measurements. The width  $W$  of the constrictions was taken as 200 nm which corresponds to the experimental gate structure. The values of  $\tau_{ac}$  and  $\tau_{pop}$  are taken to be 1.8 ns and 2.0 ps, respectively, as discussed earlier. The capacitance has not been experimentally determined. However, a good fit to the data was obtained using a value of  $1 \times 10^{-16}$  F, which is in agreement with the value inferred from similar quantum dot structures studied by Johnson *et al.*<sup>20</sup> As shown in Fig. 2, the values of  $N$ ,  $\alpha$ , and the constriction barrier  $\phi_0$  are different for the two sets of data shown. The number of particles in both cases, 170 and 155, is consistent with the expected number of particles in the dot based on the area, 2DEG density, and the lateral depletion width into the dot with gate bias. As mentioned earlier, the experimental gate geometry coupled with the depletion width gives  $\alpha \approx 3$ , and should increase with increasing negative gate bias as the depletion width grows. The zero bias barrier height  $\phi_0$  determines the maximum source drain voltage across the device, which corresponds to the switching voltage  $V_s$  used by Wu *et al.*<sup>1</sup> At very low temperature, switching from the high impedance to low impedance state occurs when the Fermi energy  $E_{F1}$  equals  $e\phi_1$  in Eq. (3), which gives (assuming  $Q \approx 0$  just before switching occurs)

$$V_s = 2\alpha \left( \phi_0 - \frac{E_{F1}}{e} \right). \quad (10)$$

As the gate bias is made more negative, the zero bias barrier  $\phi_0$  increases due to the increased depletion under the gate electrodes forming the constriction. Thus, Eq. (10) explains the increase in  $V_s$  with increasing negative gate bias shown in Fig. 3 of Wu *et al.* The fit values of 36 and 49 mV for  $\phi_0$  are consistent with the range of energies given by self-consistent envelope-function calculations for similar GaAs/Al<sub>x</sub>Ga<sub>1-x</sub>As split gate structures.<sup>21</sup>

The model shows that the system is sensitive to a num-

ber of different parameters related to the material and structure of the quantum dot. As evidenced by Eq. (10), the switching voltage is primarily determined by the zero bias barrier and  $\alpha$ . The holding voltage  $V_h$ , corresponding to  $V_{sd}$  of the low impedance state, is sensitive to parameters related to energy loss in the cavity. Of these parameters, the number of particles in the cavity  $N$  and the effective polar-optical phonon relaxation time  $\tau_{pop}$  have the most influence on the fit shown in Fig. 2. As  $N$  is decreased, and  $\tau_{pop}$  is increased, the holding voltage shifts to lower values. The data could only be fit using the longer time of  $\tau_{pop} = 2$  ps suggesting the dominance of nonequilibrium phonon effects in the energy relaxation rate.<sup>13</sup> The acoustic relaxation time was found to have very little effect on the fit. The single electron charging voltage,  $e/C \approx 1.5$  mV, is small compared to the values of  $V_{sd}$ , and thus discrete electron effects are expected to be small.

Experimentally, Wu *et al.* observed that higher lattice temperatures required higher negative gate bias to achieve NDC. In the present model, the NDC is found to disappear for the lower gate bias data [Fig. 2 curve (a)] at a temperature of about 15 K, and higher temperature for the higher bias data. This result is in close agreement with the experiments. This behavior may be understood if switching occurs when a critical current for electron heating is reached. At low temperature, this current is not attained until the condition given by Eq. (10) is reached. However, at higher temperature, the critical current is reached at lower voltage due to the exponential increase in thermionic emission current with temperature.

Figure 3 shows the change in electron temperature, and the number of electrons in the cavity as a function of the current  $I$ . The electron temperature initially rises until the temperature reaches about 50 K, at which point energy loss due to optical-phonon emission slows down the rate of increase of  $T_e$ . At high current, the effective electron temperature exceeds the lattice temperature by two orders of magnitude. The number of particles in the cavity decreases as the current and electron temperature increases. Thus,  $Q$  becomes increasingly positive as the

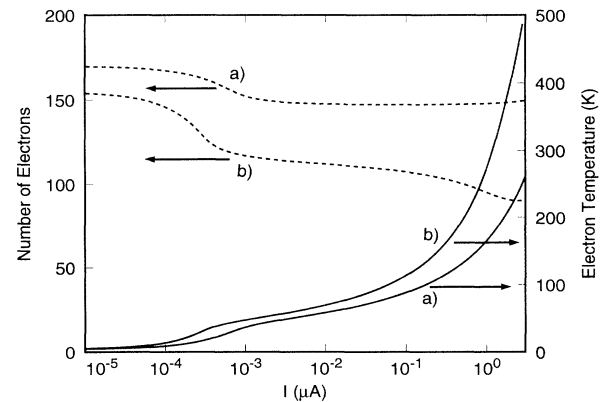


FIG. 3. The electron temperature and number of particles in the cavity vs current for the curves (a) and (b) shown in Fig. 2.

current increases, causing the voltage drop across the two barriers to become asymmetric with an increasing fraction dropped across the first barrier  $A$ .

The model presented herein shows excellent agreement with the experiment, particularly at higher negative gate biases. At lower gate bias, where the barrier heights are small compared to the Fermi energy, poorer agreement is found due to the neglect of degeneracy effects in the model. Other effects neglected in the present model which may play a role at high injection energies include occupancy of higher subbands as well as real-space trans-

fer into the  $\text{Al}_x\text{Ga}_{1-x}\text{As}$  barriers. More precise fully numerical models using, for example, Monte Carlo techniques are necessary to ascertain the effects of these non-ideal effects, as well as providing a more accurate model for energy relaxation and activation over the constriction barriers, which will be the subject of future investigation.

We wish to acknowledge the partial support by the National Science Foundation Grant No. ECS-9216768 and the Office of Naval Research, Grant No. N00014-93-1-0618.

- <sup>1</sup> J. C. Wu, M. N. Wybourne, C. Berven, S. M. Goodnick, and D. D. Smith, *Appl. Phys. Lett.* **61**, 1 (1992).
- <sup>2</sup> C. W. J. Beenakker and H. van Houten, in *Solid State Physics*, edited by H. Ehrenreich and D. Turnbull (Academic, Boston, 1991), Vol. 44, p. 1
- <sup>3</sup> R. J. Brown, M. J. Kelly, R. Newbury, M. Pepper, B. Miller, H. Ahmed, D. G. Hasko, D. C. Peacock, D. A. Ritchie, J. E. F. Frost, D. A. Ritchie, and G. A. C. Jones, *Solid State Electron.* **32**, 1179 (1989).
- <sup>4</sup> M. Heiblum and U. Sivan, in *Hot Carriers in Semiconductor Nanostructures: Physics and Applications*, edited by J. Shah (Academic Press, Boston, 1992), pp. 411–440.
- <sup>5</sup> K. Hess, T. K. Higman, M. A. Emanuel, and J. J. Coleman, *J. Appl. Phys.* **60**, 3775 (1986).
- <sup>6</sup> A. M. Belyantsev, A. A. Ignatov, V. I. Piskarev, M. A. Sinitsyn, V. I. Shashkin, B. S. Yavich, and M. L. Yakovlev, *Pis'ma Zh. Eksp. Teor. Fiz.* **43**, 339 (1986) [*JETP Lett.* **43**, 437 (1986)].
- <sup>7</sup> Zh. I. Alferov, O. A. Mezrin, M. A. Sinitsyn, S. I. Troshkov, and B. S. Yavich, *Fiz. Tekh. Poluprovodn.* **21**, 494 (1987) [*Sov. Phys. Semicond.* **21**, 304 (1987)].
- <sup>8</sup> T. K. Higman, L. M. Miller, M. E. Favaro, M. A. Emanuel, K. Hess, and J. J. Coleman, *Appl. Phys. Lett.* **53**, 1623 (1988).
- <sup>9</sup> M. A. Emanuel, T. K. Higman, J. M. Higman, J. M. Kolodzey, J. J. Coleman, and K. Hess, *Solid State Electron.* **31**, 589 (1988).
- <sup>10</sup> O. A. Mezrin and S. I. Troshkov, *Fiz. Tekh. Poluprovodn.* **20**, 1298 (1986) [*Sov. Phys. Semicond.* **20**, 819 (1986)].
- <sup>11</sup> V. I. Tolstikhin, *Fiz. Tekh. Poluprovodn.* **20**, 2199 (1986) [*Sov. Phys. Semicond.* **20**, 1375 (1986)].
- <sup>12</sup> D. Arnold, K. Hess, and G. J. Iafrate, *Appl. Phys. Lett.* **53**, 374 (1988).
- <sup>13</sup> J. Shah, A. Pinczuk, A. C. Gossard, and W. Wiegmann, *Phys. Rev. Lett.* **54**, 2045 (1985).
- <sup>14</sup> S. J. Manion, M. Artaki, M. A. Emanuel, J. J. Coleman, and K. Hess, *Phys. Rev. B* **35**, 9203 (1987).
- <sup>15</sup> D. R. Leadley, R. J. Nicholas, J. J. Harris, and C. T. Foxon, *Semicond. Sci. Technol.* **4**, 885 (1989).
- <sup>16</sup> J. K. Wigmore, M. Erol, M. Sahraoui-Tahar, M. Ari, C. E. W. Wilkinson, J. H. Davies, M. Holland, and C. Stanley, *Semicond. Sci. Technol.* **8**, 322 (1993).
- <sup>17</sup> T. Kawamura, S. Das Sarma, R. Jalabert, and J. K. Jain, *Phys. Rev. B* **42**, 5407 (1990).
- <sup>18</sup> M. E. Daniels, B. K. Ridley, and M. Emeny, *Solid State Electron.* **32**, 1297 (1989).
- <sup>19</sup> W. Pötz and P. Kocevār, in *Hot Carriers in Semiconductor Nanostructures: Physics and Applications* (Ref. 4), pp. 87–120.
- <sup>20</sup> A. T. Johnson, L. P. Kouwenhoven, W. de Jong, N. C. van der Vaart, and C. J. P. M. Harmans, *Phys. Rev. Lett.* **69**, 1592 (1992).
- <sup>21</sup> S. E. Laux, D. J. Frank, and F. Stern, *Surf. Sci.* **196**, 101 (1988).